

Nuclear fragmentation induced by low-energy antiprotons within a microscopic transport approach

Zhao-Qing Feng*

Institute of Modern Physics, Chinese Academy of Sciences, Lanzhou 730000, People's Republic of China

(Received 20 September 2016; revised manuscript received 27 October 2016; published 1 December 2016)

Within the framework of the Lanzhou quantum molecular-dynamics transport model, the nuclear fragmentation induced by low-energy antiprotons has been investigated thoroughly. A coalescence approach is developed for constructing the primary fragments in phase space. The secondary decay process of the fragments is described by a well-known statistical code. It is found that the localized energy released in antibaryon-baryon annihilation is deposited in a nucleus mainly via pion-nucleon collisions, which leads to the emissions of pre-equilibrium particles, fission, evaporation of nucleons, light fragments, etc. The strangeness exchange reactions dominate the hyperon production. The averaged mass loss increases with the mass number of target nucleus. A bump structure in the domain of intermediate mass for heavy targets appears owing to the contribution of fission fragments.

DOI: [10.1103/PhysRevC.94.064601](https://doi.org/10.1103/PhysRevC.94.064601)**I. INTRODUCTION**

The properties of highly excited nuclei (hot nuclei) have attracted much attention in past decades via heavy-ion and hadron induced nuclear reactions, which are related to many interesting issues, i.e., liquid-gas phase transition, fast fission, new isotope production, the nuclear equation of state, etc. [1–5]. The decay mechanism of the hot nuclei varies with the excitation energy. For example, particle evaporation and fission dominate the de-excitation process at the excitation energies of 1–2 MeV/nucleon, in which the nuclear structure effects are of importance, i.e., separation energy, shell effect, odd-even effect, etc. At high excitation energies, the explosive decay is pronounced via the multifragment disintegration. The mechanism has been extensively investigated in heavy-ion collisions. The fragments are produced tending to the β -stability line. The symmetry energy plays an important role in rare isotope production. A large angular momentum transit and compression of the nuclear system are undertaken in heavy-ion collisions, which complicate the formation of hot nuclei. To avoid shortcomings, hadron-nucleus collisions could be chosen for heating nuclei. A more localized energy is deposited in a nucleus in antiproton induced reactions. For example, the average excitation energy after the stopped antiproton annihilation in a Cu target is similar to the average excitation energy irradiated by a 2-GeV proton [6].

The decay mechanism of hot nuclei heated by stopped and energetic antiprotons has been investigated with the facility of the low-energy antiproton ring (LEAR) at CERN [7–11]. Some interest findings were reported, e.g., the delayed fission by antiproton annihilation in heavy nuclei [12]. The reaction dynamics induced by antiprotons is complicated and associated with the annihilation between antibaryon and baryon, charge-exchange reactions, and elastic and inelastic collisions. To understand the nuclear dynamics induced by antiprotons, several approaches have been proposed, such as the intranuclear cascade model [13], kinetic approach [14], Giessen Boltzmann-Uehling-Uhlenbeck transport

model [15,16], Statistical multifragmentation model [17], and Lanzhou quantum molecular-dynamics (LQMD) approach [18]. Antiproton-nucleus collisions provide possibilities for studying the properties of hot nuclei, meson-nucleon interactions, formation of hypernucleus, etc. It has the advantage of heating the nucleus with the excitation energy of several hundreds of MeV and with less compression of the nuclear system because of the annihilation reactions. In this work, the fragmentation mechanism in low-energy antiproton induced nuclear reactions is investigated, in which the nuclear structure effects and reaction channels are discussed.

II. BRIEF DESCRIPTION OF THE MODEL

The LQMD transport model has been successfully used for the isospin physics in heavy-ion collisions, particle production, and in-medium effects in heavy-ion and hadron (p, \bar{p}, π, K) induced reactions, hypernucleus production, etc. In the model, the production of resonances, hyperons, and mesons is coupled to hadron-hadron collisions, annihilation reactions of antibaryon-baryon collisions, decays of resonances, in-medium corrections on threshold energies, and transportation in mean-field potentials [19,20]. The temporal evolutions of baryons (nucleons, resonances, and hyperons), antibaryons, and mesons in the nuclear collisions are governed by Hamilton's equations of motion. The Hamiltonian of nucleons and nonstrangeness resonances is constructed within the Skyrme effective interaction, in which the isospin and momentum dependent potential is implemented. The Hamiltonian of hyperons (Λ, Σ , and Ξ) and pseudoscalar mesons (π, η, K , and \bar{K}) is derived from the relativistic covariant theories based on the fitting available optical potentials [20,21].

The mean-field potential of a antinucleon is composed of the G-parity transformation of nucleon self-energies with a scaling approach. The antinucleon energy in a nuclear medium is evaluated by the dispersion relation as

$$\omega_{\bar{N}}(\mathbf{p}_i, \rho_i) = \sqrt{(m_N + \Sigma_S^{\bar{N}})^2 + \mathbf{p}_i^2 + \Sigma_V^{\bar{N}}} \quad (1)$$

with $\Sigma_S^{\bar{N}} = \Sigma_S^N$ and $\Sigma_V^{\bar{N}} = -\Sigma_V^N$. The nuclear scalar Σ_S^N and vector Σ_V^N self-energies are computed from the well-

*Corresponding author: fengzqh@impcas.ac.cn

known relativistic mean-field model with the NL3 parameter ($g_{\sigma N}^2 = 80.8$, $g_{\omega N}^2 = 155$, and $g_{\rho N}^2 = 20$). The optical potential of a baryon or antibaryon is derived from the in-medium energy as $V_{\text{opt}}(\mathbf{p}, \rho) = \omega(\mathbf{p}, \rho) - \sqrt{\mathbf{p}^2 + m^2}$. A very deep antiproton-nucleus potential is obtained with the G-parity approach being $V_{\text{opt}}(\mathbf{p} = 0, \rho = \rho_0) = -655$ MeV. From fitting the antiproton-nucleus scattering [15] and the real part of the phenomenological antinucleon-nucleon optical potential [22], a factor ξ is introduced in order to moderately evaluate the optical potential as $\Sigma_S^{\bar{N}} = \xi \Sigma_S^N$ and $\Sigma_V^{\bar{N}} = -\xi \Sigma_V^N$ with $\xi = 0.25$, which leads to the strength of $V_{\bar{N}} = -164$ MeV at the normal nuclear density $\rho_0 = 0.16 \text{ fm}^{-3}$.

Besides the reaction channels associated with resonances, hyperons, and mesons in the model, the annihilation channels, charge-exchange reaction (CEX), and elastic (EL) and inelastic scattering with antibaryons are included as follows [18]:

$$\begin{aligned} \bar{B}B &\rightarrow \text{annihilation}(\pi, \eta, \rho, \omega, K, \bar{K}, \eta', K^*, \bar{K}^*, \phi), \\ \bar{B}B &\rightarrow \bar{B}B(\text{CEX}, \text{EL}), \bar{N}N \leftrightarrow \bar{N}\Delta(\bar{\Delta}N), \bar{B}B \rightarrow \bar{Y}Y. \end{aligned} \quad (2)$$

Here the B stands for the nucleon and $\Delta(1232)$, $Y(\Lambda, \Sigma, \Xi)$, $K(K^0, K^+)$, and $\bar{K}(\bar{K}^0, K^-)$. The overline of B (Y) means its antiparticle. The cross sections of these channels are based on the parametrization or extrapolation from available experimental data [23]. The annihilation dynamics in antibaryon-baryon collisions is described by a statistical model with SU(3) symmetry inclusion of all pseudoscalar and vector mesons [24], which considers various combinations of possible mesons with the final state from two to six particles [25]. Pions as the dominant products in the annihilation of the antiproton in the nucleus contribute the energy deposition.

III. RESULTS AND DISCUSSION

The particle production in antiproton induced reactions is a significant probe in understanding the in-medium properties

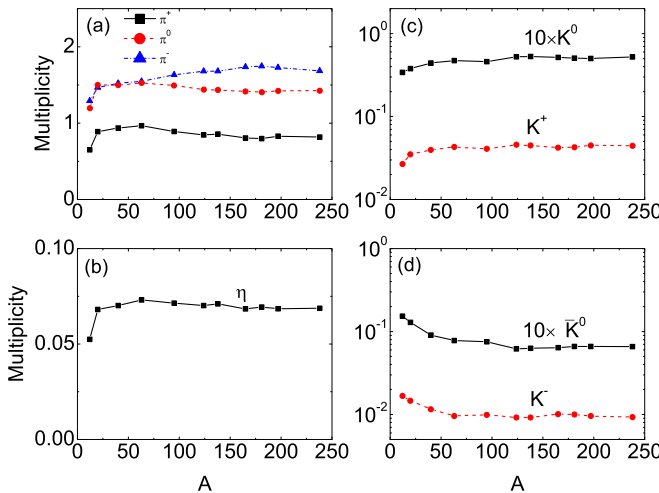


FIG. 1. Total multiplicities of pseudoscalar meson (a) pions, (b) etas, (c) kaons, and (d) antikaons as a function of mass number of target nuclei in antiproton induced reactions.

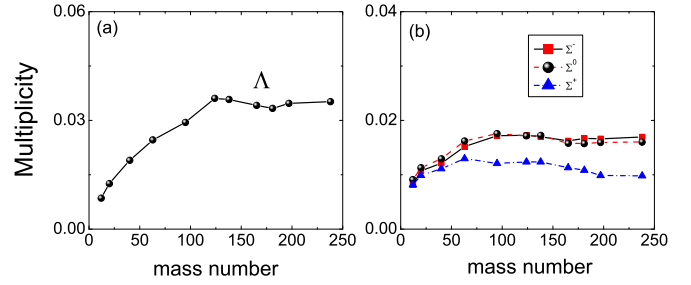


FIG. 2. The same as in Fig. 1, but for the (a) Λ and (b) Σ production.

of particles, annihilation mechanism, strangeness exchange reactions, etc. The localized energy is deposited in a target nucleus via the collisions of particles and nucleons, which makes the formation of a highly excited nucleus. The particle emission is strongly influenced by surrounding nucleons. Shown in Fig. 1 is the mass dependence of the pseudoscalar in antiproton induced reactions at an incident momentum of 200 MeV/c (kinetic energy of 21 MeV). The targets of ^{12}C , ^{20}Ne , ^{40}Ca , ^{63}Cu , ^{95}Mo , ^{124}Sn , ^{138}Ba , ^{165}Ho , ^{181}Ta , ^{197}Au , and ^{238}U are used for the bombardment with antiprotons. It is interesting that the π^- production increases with the mass of the target nucleus, which is caused from the annihilation of antiprotons on neutrons. The secondary collisions of antikaons on nucleons reduces the antikaon yields, i.e., $\bar{K}N \rightarrow \pi Y$, which contribute the production of hyperons as shown in Fig. 2. The η and kaons are insensitive to the target mass because of weakly interacting with nucleons. At the considered momentum below its threshold energy, e.g., the reaction $\bar{N}N \rightarrow \bar{\Lambda}\Lambda$ ($p_{\text{threshold}} = 1.439$ GeV/c), hyperons are mainly contributed from the secondary collisions and strangeness exchange reactions after annihilations, i.e., $\pi N \rightarrow KY$ and $\bar{K}N \rightarrow \pi Y$.

Besides the emission of mesons and hyperons after the annihilation of antiprotons in nuclei, target nuclei are excited via the collisions of particles and nucleons, which leads to evaporating nucleons and clusters from the transient nuclei and even to fragmentation reactions. The mass and charge yield distributions could be used to estimate the energy released by antiprotons in nuclei from the fragmentation magnitude. The nuclear dynamics induced by antiprotons is described by

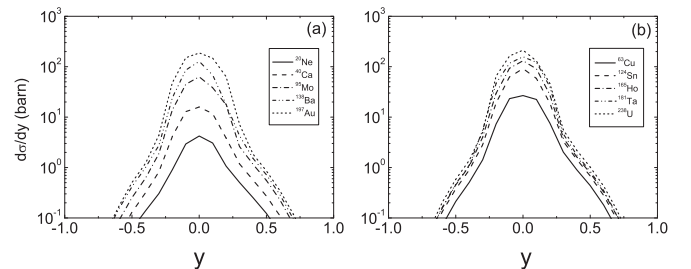


FIG. 3. Rapidity distributions of light complex particles (nucleons, hydrogen, and helium isotopes) in antiproton induced reactions on the nuclei of (a) ^{20}Ne , ^{40}Ca , ^{95}Mo , ^{138}Ba , ^{197}Au and (b) ^{63}Cu , ^{124}Sn , ^{165}Ho , ^{181}Ta , ^{238}U at the momentum of 200 MeV/c.

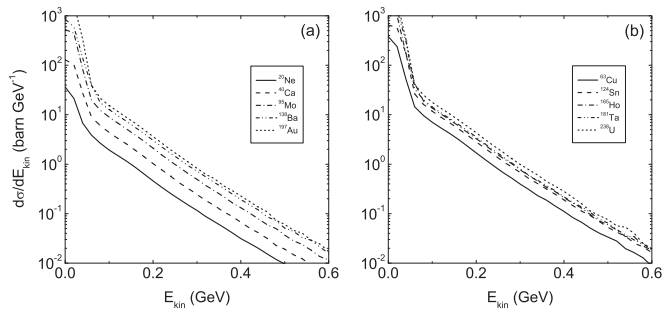
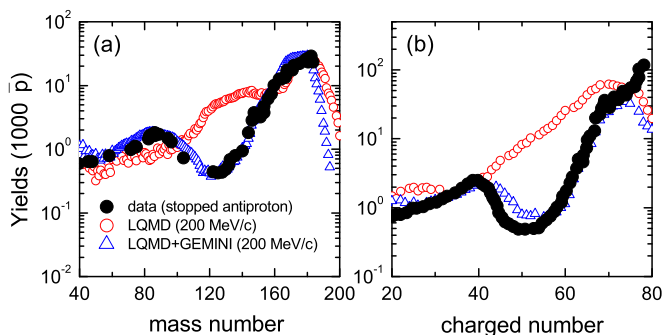
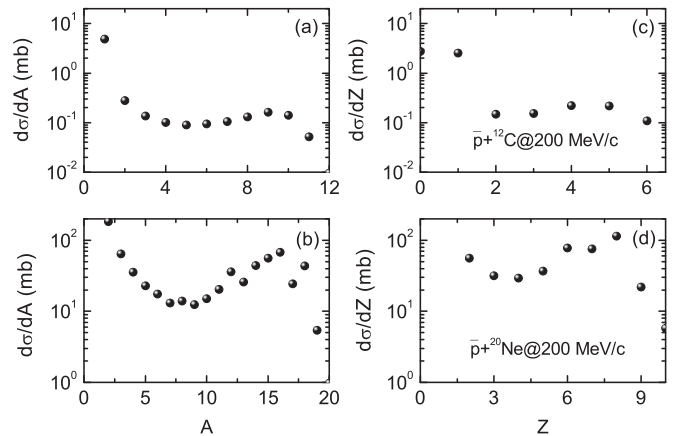


FIG. 4. The same as in Fig. 3, but for the kinetic-energy spectra.

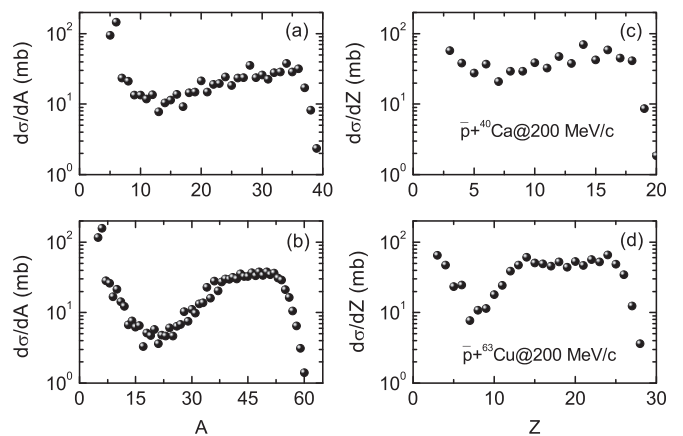
the LQMD model. The primary fragments are constructed in phase space with a coalescence model, in which nucleons at the freeze-out stage (equilibrium state for particle production) are considered to belong to one cluster with the relative momentum smaller than P_0 and with the relative distance smaller than R_0 (here $P_0 = 200$ MeV/c and $R_0 = 3$ fm). The primary fragments are highly excited. The de-excitation of the fragments is assumed to be isolated without rotation (zero angular momentum) and evaluated with the statistical code GEMINI [26]. The phase-space distributions of fragments manifest the excitation magnitude of the target nucleus. The rapidity and kinetic-energy spectra of light clusters ($Z \leq 2$) are presented as shown in Figs. 3 and 4, respectively. The shapes of different targets are very similar, which means the nuclear structure effects (separation energy, shell effect, pairing correlation, etc.) are negligible in the antiproton induced reactions.

The fragmentation reactions induced by antiprotons were investigated in experiments at the LEAR at CERN. The energy deposition mechanism and properties of highly excited nuclei are concentrated on. The combined approach is tested in the fragmentation reactions of antiprotons on ^{197}Au as shown in Fig. 5. The available data from the LEAR facility [27] could be nicely reproduced within the LQMD model combined with the GEMINI code. It is obvious that the primary fragments in the mass region of $100 < A < 160$ are highly excited and the yields are overestimated. The secondary decay leads


 FIG. 5. (a) Mass spectra and (b) charge distributions of fragments produced in the $\bar{p} + ^{197}\text{Au}$ reaction at an incident momentum of 200 MeV/c combined with the statistical decay code GEMINI. The mass yields from the LEAR facility at CERN [27] are shown for comparison.

 FIG. 6. Fragment distributions in antiproton induced reactions at the incident momentum of 200 MeV/c as functions of (a) mass number on ^{12}C , (b) mass number on ^{20}Ne , (c) charged number on ^{12}C , and (d) charged number on ^{20}Ne , respectively.

to the appearance of a bump structure around $A \sim 90$, which comes from the fission of heavy fragments. The minimum position of the yields appears at $A \sim 120$ and $Z \sim 50$ and the yields increase drastically with the fragments becoming heavier. Overall, the available data could be reproduced within the LQMD transport model combined with the GEMINI code. Moreover, based on the combined approach, I analyzed the fragmentation reactions with antiprotons at the incident momentum of 200 MeV/c on the light nuclei of ^{12}C , ^{20}Ne , ^{40}Ca , and ^{63}Cu as shown in Figs. 6 and 7, respectively. A broad region of targetlike nuclei is formed and the structure is similar, where the fragments are produced via the pre-equilibrium particle emission and evaporation from the hot nuclei. The fragmentation process can be understood as three stages, namely, antiproton-nucleon annihilation (energy released), meson-nucleon collisions (energy deposited), and fragmentation of a highly excited nucleus (nuclear explosion).

The fragmentation process of the target nucleus induced by the antiproton undergoes the explosive process (fast stage)


 FIG. 7. The same as in Fig. 6, but for (a) mass number on ^{40}Ca , (b) mass number on ^{63}Cu , (c) charged number on ^{40}Ca , and (d) charged number on ^{63}Cu , respectively.

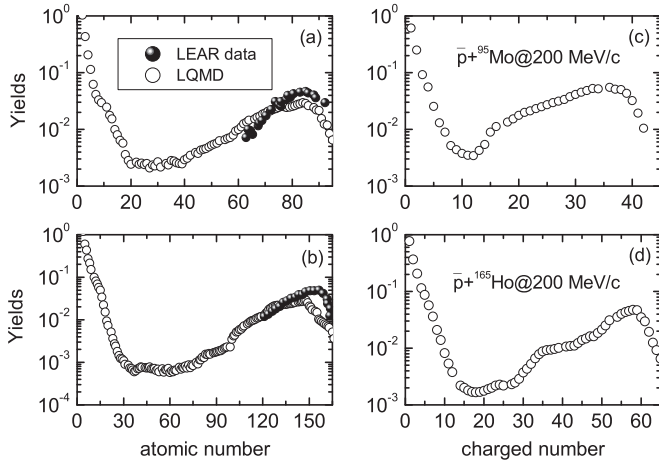


FIG. 8. Fragmentation reactions induced by antiprotons and compared with the LEAR data [28] for the fragment (a) mass on ^{95}Mo , (b) mass on ^{165}Ho , (c) charged number ^{95}Mo , and (d) charged number distributions on ^{165}Ho , respectively.

in which the pre-equilibrium nucleons (light clusters) are emitted or the multifragments are produced after collisions between baryons and nucleons, and the decay process (slow stage) of the highly excited nucleus after the relative motion energy is deposited via the meson-nucleon collisions. The decay mechanism is determined by the excitation energy, i.e., the particle evaporation or fission dominating at low excitation energies (1–2 MeV/nucleon). The system is broken via multifragmentation when the local energy is close to the binding energy. More sophisticated investigations on the fragmentation reactions are performed. Shown in Fig. 8 is the mass (left window) and charge (right window) distributions of fragments compared with the LEAR data with stopped antiprotons [28]. The production yields per antiproton are consistent with the available data. The average excitation energies are 157 and 415 MeV for the target nuclei ^{95}Mo and ^{165}Ho , respectively, which are evaluated from the formula of $\langle E^* \rangle = \int E^* \sigma(E^*) dE^* / \int \sigma(E^*) dE^*$, $\sigma(E^*)$ being the sum of cross sections of fragments at the excitation energy of E^* . The multifragmentation into intermediate mass fragments (IMFs) ($3 < Z < 30$) is negligible because of the limitation of excitation energy. Similar structures on the targets of ^{124}Sn and ^{138}Ba are found in Fig. 9 with the excitation energies of 238 and 288 MeV, respectively. Roughly, the deposited energy increases with the mass of the target nucleus, but weakly depends on the incident energy. Contribution of the fission fragments on the spectra is pronounced with the heavy target as shown in Fig. 10, in particular for ^{238}U .

The mean nucleon removal in antiproton induced reactions manifests the meson-nucleon collision probability and is also related to the deposited energy in the nucleus. The average mass removals are evaluated from $\Delta A = A_T - 1 - \int_{A_{\min}}^{A_T-2} \sigma(A) dA / \int_{A_{\min}}^{A_T-2} \sigma(A) dA$. Here, the A_T and A_{\min} are the mass number of the target nucleus and the integration limit being the first minimum position from the targetlike fragments. Shown in Fig. 11 is a comparison of calculated removal nucleon number and the available data from the LEAR facility

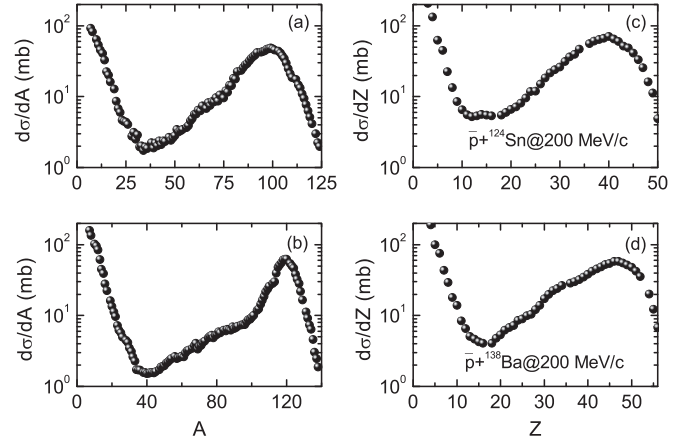


FIG. 9. Fragment distributions in the antiproton induced reactions for the spectra of mass (a) ^{124}Sn and (b) ^{138}Ba and charge number (c) ^{124}Sn and (d) ^{138}Ba , respectively.

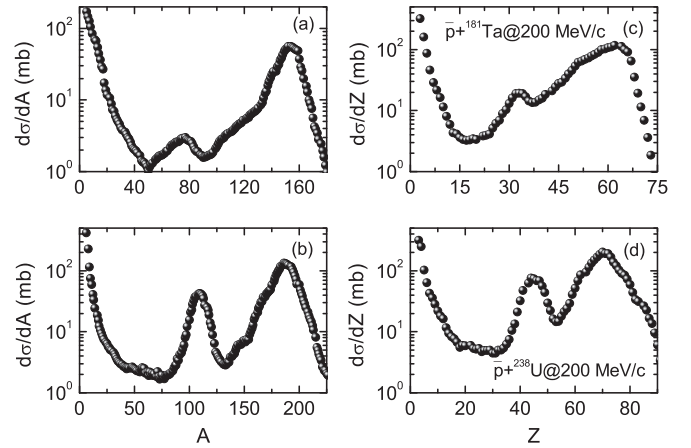


FIG. 10. The same as in Fig. 9, but for the mass distributions on (a) ^{181}Ta and (b) ^{238}U as well as charge spectra on (c) ^{181}Ta and (d) ^{238}U , respectively.

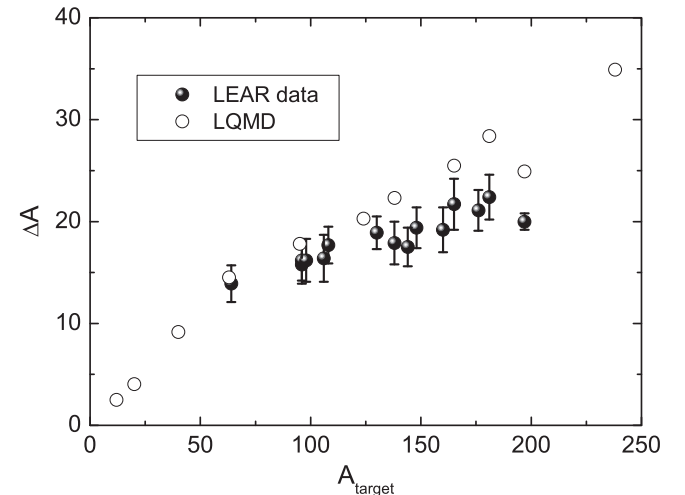


FIG. 11. Averaged mass removal as a function of mass number of target nuclei [27].

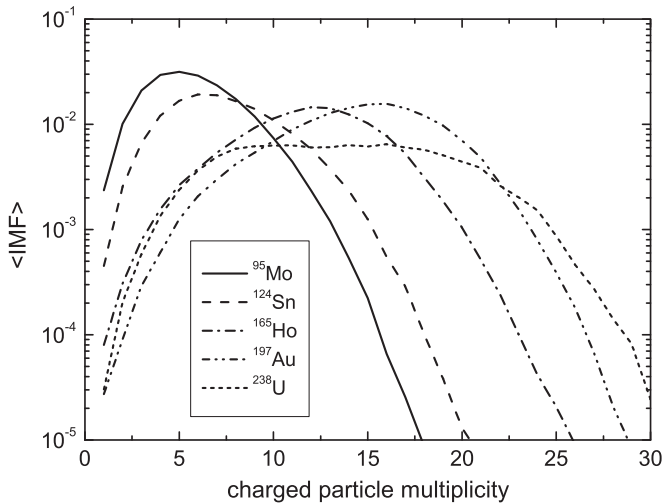


FIG. 12. Correlation of the intermediate mass fragments (IMFs) and charged particle multiplicity produced in \bar{p} induced reactions on different targets.

[27]. Reactions on the targets of ^{12}C , ^{20}Ne , ^{40}Ca , ^{63}Cu , ^{95}Mo , ^{124}Sn , ^{138}Ba , ^{165}Ho , ^{181}Ta , ^{197}Au , and ^{238}U with antiprotons at the incident momentum of 200 MeV/c are performed. The removal nucleons increase with the target nuclei because of the larger meson-nucleon collision probabilities for heavier nuclei. The averaged particle emission is related to the excitation energy. For example, on average 17.8 nucleons are emitted from the target ^{95}Mo , and including 3.1 nucleons from the pre-equilibrium stage. Therefore, 14.7 nucleons evaporated from the thermal system and assuming the 8-MeV separation energy and 3-MeV kinetic energy per nucleon [29] leads to the excitation energy of 161.7 MeV. The value is close to the evaluation from the energy spectra (157 MeV).

The IMFs produced in Fermi-energy heavy-ion collisions has been investigated for extracting the nuclear equation of state, liquid-gas phase transition, and density dependence of

symmetry energy [30,31], where the composite system is formed at excitation energies of 10–20 MeV per nucleon. The fluctuation and explosive decay of the excited system contribute the IMF production. Shown in Fig. 12 is the correlation of the IMF multiplicity and charged particles on the targets of ^{95}Mo , ^{124}Sn , ^{165}Ho , ^{197}Au , and ^{238}U with antiprotons at the incident momentum of 200 MeV/c. A broad distribution is found for the heavier target. The IMF production in antiproton induced reactions is strongly compressed in comparison to heavy-ion collisions owing to less fluctuation and lower excitation energy.

IV. CONCLUSIONS

The fragmentation reaction induced by low-energy antiprotons has been investigated within the LQMD transport model. The de-excitation of the primary fragments is described with the help of the statistical code GEMINI. The available data of the fragment production from the LEAR at CERN can be nicely reproduced with the combined approach. The energy released in the antiproton-nucleon annihilation is mainly deposited in the target nucleus via the pion-nucleon collisions. The averaged nucleons removed from the target nucleus increase with the mass number. The bump structure contributed from the fission fragments of heavy nuclei is observed. Hyperons are mainly produced via strangeness exchange reactions in collisions of antikaons and nucleons, which have smaller relative momentum and could be easily captured by the residue nuclei to form hypernuclei. The approach will provide a cornerstone for the antiproton physics at PANDA (Antiproton Annihilation at Darmstadt, Germany) in the near future, i.e., hypernuclei, in-medium properties of hadrons, etc.

ACKNOWLEDGMENTS

This work was supported by the Major State Basic Research Development Program in China (Grant No. 2015CB856903) and the National Natural Science Foundation of China (Grants No. 11675226 and No. 11175218).

-
- [1] P. Chomaz, M. Colonna, and J. Randrup, *Phys. Rep.* **389**, 263 (2004).
- [2] M. Colonna, M. Di Toro, A. Guarnera, V. Latora, and A. Smerzi, *Phys. Lett. B* **307**, 273 (1993); M. Colonna, M. Di Toro, and A. Guarnera, *Nucl. Phys. A* **580**, 312 (1994).
- [3] J. Pochodzalla, T. Mohlenkamp, T. Rubehn, A. Schuttauf, A. Worner, E. Zude, M. Begemann-Blaich, T. Blaich, H. Emling, A. Ferrero, C. Gross, G. Imme, I. Iori, G. J. Kunde, W. D. Kunze, V. Lindenstruth, U. Lynen, A. Moroni, W. F. J. Muller, B. Ocker, G. Raciti, H. Sann, C. Schwarz, W. Seidel, V. Serfling, J. Stroth, W. Trautmann, A. Trzcinski, A. Tucholski, G. Verde, and B. Zwieglinski, *Phys. Rev. Lett.* **75**, 1040 (1995).
- [4] H.-Y. Wu, G.-X. Dai, G.-M. Jin *et al.*, *Phys. Rev. C* **57**, 3178 (1998); H.-Y. Wu *et al.*, *Phys. Lett. B* **538**, 39 (2002).
- [5] Y. G. Ma, *Phys. Rev. Lett.* **83**, 3617 (1999).
- [6] J. Jastrzebski, W. Kurcewicz, P. Lubinski, A. Grabowska, A. Stolarz, H. Daniel, T. von Egidy, F. J. Hartmann, P. Hofmann, Y. S. Kim, A. S. Botvina, Y. S. Golubeva, A. S. Iljinov, G. Riepe, and H. S. Plendl, *Phys. Rev. C* **47**, 216 (1993).
- [7] T. von Egidy *et al.*, *Z. Phys. A* **335**, 451 (1990).
- [8] P. Hofmann, A. S. Iljinov, Y. S. Kim, M. V. Mebel, H. Daniel, P. David, T. von Egidy, T. Haninger, F. J. Hartmann, J. Jastrzebski, W. Kurcewicz, J. Lieb, H. Machner, H. S. Plendl, G. Riepe, B. Wright, and K. Ziock, *Phys. Rev. C* **49**, 2555 (1994).
- [9] Y. S. Kim, A. S. Iljinov, M. V. Mebel, P. Hofmann, H. Daniel, T. von Egidy, T. Haninger, F. J. Hartmann, H. Machner, H. S. Plendl, and G. Riepe, *Phys. Rev. C* **54**, 2469 (1996).
- [10] U. Jahnke, W. Bohne, T. von Egidy, P. Figuera, J. Galin, F. Goldenbaum, D. Hilscher, J. Jastrzebski, B. Lott, M. Morjean, G. Pausch, A. Peghaire, L. Pienkowski, D. Polster, S. Proschitzki, B. Quednau, H. Rossner, S. Schmid, and W. Schmid, *Phys. Rev. Lett.* **83**, 4959 (1999).
- [11] B. Lott, F. Goldenbaum, A. Bohm, W. Bohne, T. von Egidy, P. Figuera, J. Galin, D. Hilscher, U. Jahnke, J. Jastrzebski,

- M. Morjean, G. Pausch, A. Peghaire, L. Pienkowski, D. Polster, S. Proschitzki, B. Quednau, H. Rossner, S. Schmid, and W. Schmid, *Phys. Rev. C* **63**, 034616 (2001).
- [12] J. P. Bocquet *et al.*, *Phys. Lett. B* **182**, 146 (1986); **192**, 312 (1987).
- [13] J. Cugnon, P. Deneye, and J. Vandermeulen, *Nucl. Phys. A* **500**, 701 (1989); *Phys. Rev. C* **41**, 1701 (1990).
- [14] C. M. Ko and R. Yuan, *Phys. Lett. B* **192**, 31 (1987).
- [15] A. B. Larionov, I. A. Pshenichnov, I. N. Mishustin, and W. Greiner, *Phys. Rev. C* **80**, 021601(R) (2009); A. B. Larionov, *Nucl. Sci. Tech.* **26**, S20506 (2015) (in Chinese).
- [16] T. Gaitanos, A. B. Larionov, H. Lenske, and U. Mosel, *Nucl. Phys. A* **881**, 240 (2012).
- [17] J. P. Bondorf, A. S. Botvina, A. S. Iljinov, I. N. Mishustin, and K. Sneppen, *Phys. Rep.* **257**, 133 (1995).
- [18] Z. Q. Feng and H. Lenske, *Phys. Rev. C* **89**, 044617 (2014); Z. Q. Feng, *Nucl. Sci. Tech.* **26**, S20512 (2015) (in Chinese); *Phys. Rev. C* **93**, 041601(R) (2016).
- [19] Z. Q. Feng, *Phys. Rev. C* **84**, 024610 (2011); **85**, 014604 (2012); *Nucl. Phys. A* **878**, 3 (2012); *Phys. Lett. B* **707**, 83 (2012).
- [20] Z. Q. Feng, *Phys. Rev. C* **87**, 064605 (2013); *Nucl. Phys. A* **919**, 32 (2013).
- [21] Z. Q. Feng, W. J. Xie, P. H. Chen, J. Chen, and G. M. Jin, *Phys. Rev. C* **92**, 044604 (2015).
- [22] J. Côté, M. Lacombe, B. Loiseau, B. Moussallam, and R. Vinh Mau, *Phys. Rev. Lett.* **48**, 1319 (1982).
- [23] O. Buss *et al.*, *Phys. Rep.* **512**, 1 (2012).
- [24] E. S. Golubeva, A. S. Iljinov, B. V. Krippa, and I. A. Pshenichnov, *Nucl. Phys. A* **537**, 393 (1992).
- [25] A. B. Larionov, T. Gaitanos, and U. Mosel, *Phys. Rev. C* **85**, 024614 (2012).
- [26] R. J. Charity *et al.*, *Nucl. Phys. A* **483**, 371 (1988).
- [27] P. Lubinski, A. Grochulska, T. von Egidy, K. Gulda, F. J. Hartmann, J. Jastrzebski, W. Kurcewicz, L. Pienkowski, A. Stolarz, and A. Trzcinska, *Phys. Rev. C* **66**, 044616 (2002).
- [28] E. F. Moser *et al.*, *Z. Phys. A* **333**, 89 (1989).
- [29] D. Polster, D. Hilscher, H. Rossner, T. von Egidy, F. J. Hartmann, J. Hoffmann, W. Schmid, I. A. Pshenichnov, A. S. Iljinov, Y. S. Golubeva, H. Machner, H. S. Plendl, A. Grochulska, J. Jastrzebski, W. Kurcewicz, P. Lubinski, J. Eades, and S. Neumaier, *Phys. Rev. C* **51**, 1167 (1995).
- [30] T. X. Liu, M. J. van Goethem, X. D. Liu *et al.*, *Phys. Rev. C* **69**, 014603 (2004); M. A. Famiano, T. Liu, W. G. Lynch, M. Mocko, A. M. Rogers, M. B. Tsang, M. S. Wallace, R. J. Charity, S. Komarov, D. G. Sarantites, L. G. Sobotka, and G. Verde, *Phys. Rev. Lett.* **97**, 052701 (2006).
- [31] Z. Q. Feng, *Phys. Rev. C* **94**, 014609 (2016).